Anomalous particle pinch and scaling of $\mathbf{v_{in}/D}$ based on transport analysis and multiple regression

G. Becker and O. Kardaun

Max-Planck-Institut für Plasmaphysik, Euratom-IPP Association, Garching, Germany

Abstract

Predictions of density profiles in current tokamaks and ITER require a validated scaling relation for v_{in}/D where v_{in} is the anomalous inward drift velocity and D is the anomalous diffusion coefficient. Transport analysis is necessary for determining the anomalous particle pinch from measured density profiles and for separating the impact of particle sources. A set of discharges in ASDEX Upgrade, DIII-D, JET and ASDEX is analysed using a special version of the 1.5-D BALDUR transport code. Profiles of $\rho_s v_{in}/D$ with ρ_s the effective separatrix radius, five other dimensionless parameters and many further quantities in the confinement zone are compiled, resulting in the dataset VIND1.dat, which covers a wide parameter range. Weighted multiple regression is applied to the ASDEX Upgrade subset which leads to a two-term scaling $\rho_s v_{in}(x')/D(x') = 0.0432\left[(L_{T_e}(\bar{x}')/\rho_s)^{-2.58} + 7.13\, U_L^{1.55} \nu_{e*}(\bar{x}')^{-0.42}\right] x'$ with $x' = \rho/\rho_s$, effective radius ρ and average value $\bar{x}'$. The rmse value of the scaling equals 15.2 %. The electron temperature gradient length L_{T_e} is the key parameter of the anomalous particle pinch which yields the main contribution. A further parameter is the loop voltage U_L which introduces the electron collisionality parameter ν_{e*}. All exponents are statistically significant. The parameters U_L and ν_{e*} suggest a new anomalous particle pinch term driven by the Ohmic inductive electric field. The nonlinearities in the two-term scaling show that quasilinear theory is disproved by experiment. Regression analysis of the whole dataset VIND1.dat from four tokamaks shows that the L_{T_e}/ρ_s scaling covers the dependence of $\rho_s v_{in}/D$ on the effective plasma radius. It is further found that the $\rho_s v_{in}/D$ values from transport analysis do not respond to a change in collisionality regime and are not clearly related to the prevailing turbulence type. The new scaling law predicts for ITER high values of $\rho_s v_{in}/D$ and peaked density profiles, caused by the L_{T_e}/ρ_s term and central heating due to alpha particles. The density peaking improves the energy confinement by some 20 %.

PACS numbers: 52.55.Fa, 52.25.-b, 52.25.Fi, 52.55.Dy, 02.50.-r, 02.50.Sk

1. Introduction

The shape of density profiles in a fusion reactor and in reactor-grade devices is of particular importance for their operation. Predicting the density profiles in ITER [1] by transport simulations requires a validated scaling relation for the ratio v_{in}/D where v_{in} is the anomalous inward drift velocity and D is the anomalous diffusion coefficient. Such scaling was recently developed by transport analysis and simulations and has been successfully applied to ASDEX

Upgrade, DIII-D, JET and ASDEX discharges in [2]. The present paper extends this work by a multi-dimensional statistical analysis. A dataset for the anomalous particle pinch, five dimensionless parameters and many other quantities has been assembled and analysed by regression. Our main objective is to develop a scaling relation for $\rho_s v_{in}/D$ based on transport analysis and multiple regression.

The anomalous particle flux can be written as the sum of diffusion and inward drift terms

$$\Gamma = -D\nabla n_e - n_e v_{in} \tag{1}$$

In tokamak plasmas, the anomalous transport is predominant, so that the particle balance and density profiles are primarily determined by the anomalous diffusion, anomalous particle pinch and particle sources. Analysis of nonstationary particle transport is the only method to separate these contributions. Transport analysis during the flat-top phase of the line-average density does not allow to determine D and v_{in} separately. It is possible, however, to distinguish between effects due to particle sources and v_{in}/D and to determine with sufficient accuracy the ratio v_{in}/D from measured density profiles. At low and medium densities, the effect of the particle sources due to beam fuelling and ionization of neutral gas on the density profile shape is important [2]. It was demonstrated in [2] that at a line-average density $\bar{n}_e = 5 \times 10^{19}\,\mathrm{m}^{-3}$ the beam fuelling alone ($v_{in} = 0$) already yields peaked density profiles. Thus, studies attempting to evaluate the anomalous particle pinch directly from measured density profiles lead to erroneous results and wrong conclusions, if the particle sources are not negligibly small. The impact of particle sources on the density profile becomes small only, if unrealistically high diffusion coefficients are taken [2].

Section 2 describes the transport model and code applied. In section 3, profiles of $\rho_s v_{in}/D$, five other dimensionless parameters and many further quantities are determined by transport analysis of a set of discharges from ASDEX Upgrade and other tokamaks and are compiled in a dataset. In section 4, a statistical analysis of this dataset is carried out and multiple regression is applied to develop a scaling relation for $\rho_s v_{in}/D$. Section 5 gives a summary of results and the conclusions.

2. Transport model and code

The simulations are carried out with a specially developed version of the 1.5 dimensional (1.5-D) BALDUR transport code [3, 4] which also includes a modelling of the Scrape-Off Layer (SOL) [4]. In all calculations, the Ware pinch is taken into account. Empirical anomalous electron and ion heat diffusivities χ_e and χ_i, an effective heat diffusivity $\chi = 0.5(\chi_e + \chi_i)$ and an empirical anomalous diffusion coefficient D as well as an anomalous inward drift velocity v_{in} are used. In the confinement zone, the comprehensive χ scaling for ELMy H-mode plasmas from [5] is applied, which is compatible with the global scaling ITERH92-P(y) [6]:

$$\begin{aligned}\chi_e(x) = \chi(x) = \alpha_H B_t^{-5/2} n_e(x)^{3/4} T_e(x) |\nabla T_e(x)|^{1/2} \\ \times\, q(x)^{9/4} \varepsilon(x)^{7/8} \kappa(x)^{-2} A_i^{-1} A^{-1/8} a^{-1/2}\ \left(\mathrm{m^2 s^{-1}}\right)\end{aligned} \tag{2}$$

$$D(x) = 0.6\chi_e(x) \tag{3}$$

$$v_{in}(x) = C_v \frac{2x}{\rho_w x_s^2} D(x)\ \left(\mathrm{ms}^{-1}\right) \tag{4}$$

$$\chi_i(x) = \chi_e(x) \tag{5}$$

with $\alpha_H = 3.08$, B_t in T, n_e in 10^{19} m^{-3}, T_e in keV, ∇T_e in keVm^{-1} and the half-width of the separatrix in the midplane a in m. The remaining quantities safety factor $q = q_\psi$, local toroidicity $\varepsilon = r/R$ (with r the minor half-axis of a flux surface and R the major radius), local elongation κ, hydrogenic atomic mass number A_i and aspect ratio $A = R/a$ are dimensionless. The coordinate x is equal to ρ/ρ_w with ρ the effective radius of a flux surface (in meters) and ρ_w the effective radius of the wall contour. It should be mentioned that for ASDEX Upgrade the scaling in equation (2) works as well as the more recently developed scaling law for χ, reported in [7], which is compatible with the global scaling ITERH-98P(y, 2), see [8] (chapter 2, section 6.3.1.) and [9]. The relation between D and χ_e in equation (3) results for $\chi_i = \chi_e$ (see equation (5)) from $D = 0.3(\chi_e + \chi_i)$ which is supported by the ratio of the experimental particle and energy confinement times. As indicated in [2], the $D/(\chi_e + \chi_i)$ ratio was also found to be compatible with gas oscillation analyses of D and v_{in} in ASDEX and ASDEX Upgrade discharges and was obtained in simulations of nonstationary particle transport. In equation (4), C_v is a dimensionless factor and $x_s = \rho_s/\rho_w$ with ρ_s the effective separatrix radius. The relation for v_{in} is applied in the confinement zone, while a strongly rising v_{in}/D profile is used in the edge region [2, 10]. This special treatment is required to simulate the strong density decline in the steep gradient zone measured by Thomson scattering with high spatial resolution [10].

Temperature 'pedestals' of the H-mode plasmas are modeled by applying thermal diffusivities χ_e and χ_i in the steep gradient zone which are reduced relative to the χ_e values from equation (2) [11]. In the simulations, the width of the steep gradient zone is taken to be 4 cm, as observed experimentally.

For $x < x_{q=1}$, the coefficients χ_e, χ_i, D and D_I are enhanced by adding $D_B f_q$ which, in a time averaged manner, takes into account the higher transport due to sawteeth. Here, D_B is the Bohm diffusion coefficient and $f_q \propto [(1-q)/q]^2$, see [3].

In the SOL, a transport model is used that treats separately the conductive and convective heat losses to the target plates [4]. The cross-field transport coefficients are set to be $\chi_e = \chi_i = 1.5$ m^{2}s^{-1}, $D = D_I = 0.9$ m^{2}s^{-1} and $v_{in} = v_{in,I} = 10.0$ ms^{-1}. These values are consistent with the measured temperature and density fall-off lengths in the SOL.

Trapped electron effects on the resistivity are taken into account in the confinement zone. The impurity radiation model for carbon and oxygen solves rate equations for all ionization stages and applies the anomalous transport coefficients of the main plasma also to the impurities ($D_I = D$, $v_{in,I} = v_{in}$).

During the Ohmic (OH) phase of each discharge, an Ohmic χ_e scaling is used, as given in Refs [12, 13]. The L mode discharges are modeled with heat diffusivities which are enhanced by a factor of 2 relative to χ_e from equation (2). The evolution of the measured line-average density is prescribed in the simulation and a density feedback is employed to control the influx of hydrogenic atoms. A Monte Carlo model is applied to compute the neutral density required for calculating the particle source due to ionization of neutral gas [3].

As documented in [3], neutral-beam injection is treated by computing fast ion guiding-center distributions with a Fokker-Planck code. The source function is calculated by following the fast neutrals by means of a Monte Carlo code.

3. Generation of anomalous particle pinch dataset by transport analysis

To establish the dataset described in this section, transport analysis of deuterium and hydrogen discharges from ASDEX Upgrade and deuterium discharges from DIII-D, JET and ASDEX is applied. The analysis is carried out during the flat-top phases of current and line-average density which allows to determine the ratio v_{in}/D. By contrast, evaluating the coefficients D and v_{in} separately would require an analysis of nonstationary particle transport. Results from transport simulations are taken at the 46 time slices of the discharges, given in tables 1 to 3, and at 7 radial locations in the confinement zone in the range $0.46 \leq x = \rho/\rho_w \leq 0.68$. The corresponding range for the coordinate $x' = \rho/\rho_s$, which is usually used in modellings that do not include the SOL, is $0.53 \leq x' \leq 0.78$. The profile data, comprising $\rho_s\, v_{in}/D$, five other relevant dimensionless parameters (see equation (7)) and many further quantities, are included in the anomalous particle pinch dataset VIND1.dat. This dataset covers a wide range in the dimensionless parameters and the other quantities and is used for our statistical analysis.

The ASDEX Upgrade discharges (R = 1.65 m, a = 0.5 m and κ_a = 1.6) analysed are deuterium shots with neutral beam injection ($D^0 \rightarrow D^+$) and Ohmic heating (see table 1) and hydrogen shots with neutral beam injection ($H^0 \rightarrow H^+$) and Ohmic heating (see table 2). In order to achieve a significant variation of the electron temperature profile shape, the change in the electron heating profile must be sufficiently strong. A significant peaking of the electron heating profile takes place when proceeding from NBI to ICRH, ECRH and OH. In this sequence, the measured electron temperature profile was shown to become narrower in [2], so that the electron temperature gradient length, $L_{T_e} = -T_e/\nabla T_e$, decreases. Ohmic heating during the current flat top is more central than electron heating by NBI in deuterium, yielding L_{T_e} values that are about two times smaller. In hydrogen discharges, electron heating due to NBI is more central than in deuterium, so that smaller L_{T_e} values result, too. In order to further extend the parameter range, transport analysis of the deuterium discharges in DIII-D, JET [8, 14] and ASDEX, given in table 3, is carried out. In tables 1 to 3, also the confinement mode and collisionality regime of the discharges are included. Moreover, in tables 1 and 2 the prevailing turbulence type in the plasma is classified according to the criteria given at the end of section 3.

Table 1. Parameters of deuterium discharges in ASDEX Upgrade analysed by transport simulations and included into the anomalous particle pinch dataset VIND1.dat. The banana, plateau and collisional regimes are denoted by B, P and PS, respectively. Type classifies the TEM (trapped electron mode), ITG (ion temperature gradient) and η_i mode turbulence.

Shot No	Mode	Time (s)	$\bar{n}_e$ $(10^{19}\mathrm{m}^{-3})$	I_p (MA)	B_t (T)	P_{inj} (MW)	C_v	Re-gime	Type
13309	H	2.3	5.0	1.0	2.0	2.5	0.25	B	ITG
13309	H	3.6	5.0	1.0	2.0	4.8	0.20	B	TEM
13313	H	4.5	8.9	0.8	2.0	4.8	0.25	B/P	ITG
13298	H	2.8	7.4	0.8	2.0	4.8	0.30	B	ITG
13298	H	4.5	10.0	0.8	2.0	4.8	0.20	P	ITG
13476	H	3.6	11.8	1.0	2.0	5.0	0.25	B	ITG
13588	H	2.8	5.1	1.0	2.0	2.5	0.25	B	ITG
16949	L	1.2	4.8	0.8	2.0	2.5	0.25	B	ITG
13141	OH	2.0	3.1	0.6	2.0	0.0	1.10	B/P	η_i mode
13350	OH	4.2	6.3	0.6	2.0	0.0	1.10	P/PS	η_i mode
14242	OH	1.3	3.8	1.0	2.0	0.0	1.00	B	TEM
14243	OH	1.3	3.7	1.0	2.0	0.0	1.00	B	TEM
14902	L	4.0	5.1	1.0	2.7	1.4	0.50	B	TEM/ITG
14906	L	4.0	4.7	1.0	2.7	1.4	0.50	B	TEM/ITG
14518	H	4.5	8.9	0.8	2.0	9.7	0.25	B	ITG
14519	H	3.5	8.9	0.8	2.0	9.7	0.25	B	ITG
14520	H	3.3	8.4	0.8	2.0	9.7	0.25	B	ITG
14521	H	4.0	9.0	0.8	1.7	9.8	0.25	B	ITG
14831	H	4.5	7.5	0.8	1.7	9.7	0.25	B	ITG

The L_{T_e} values in beam-heated deuterium shots are found to vary too little to determine accurately the dependence of C_v and $\rho_s\, v_{in}/D$ on L_{T_e}. It is thus necessary to include OH plasmas and hydrogen discharges with smaller L_{T_e} values. Transport analysis is carried out during the flat-top phases of current and line-average density. In selecting the discharges for the dataset, the main objective was to extend the range of plasma parameters. A wide parameter range is covered by the shots in tables 1 to 3: line-average electron density $\bar{n}_e = 2.4-11.8\times10^{19}$ m^{-3}, plasma current $I_p = 0.4-2.6$ MA, toroidal magnetic field $B_t = 1.5-2.7$ T and neutral injection heating power $P_{inj} = 1.4-17.5$ MW. Most of the shots selected are backed by other ones, which are almost identical. The data from ASDEX Upgrade displayed in tables 1 and 2 are well-conditioned with respect to $\bar{n}_e$, I_p, B_t and P_{inj}, each of which varies over a wide range. Discharges with ICRH and ECRH were not simulated and not included in the dataset. The line-average density of the ECRH shots in ASDEX Upgrade ($\bar{n}_e \simeq 2.2\times10^{19}$ m^{-3}) is too low for applying the effective χ scaling of equation (2), see [5]. Moreover, when assembling the dataset, discharges with ITB (internal transport barrier), improved H-mode and NTMs (neoclassical tearing modes) were intentionally not included.

Table 2. Parameters of hydrogen discharges in ASDEX Upgrade analysed by transport simulations and included into the dataset VIND1.dat.

Shot No	Mode	Time (s)	$\bar{n}_e$ $(10^{19}\,\mathrm{m}^{-3})$	I_p (MA)	B_t (T)	P_{inj} (MW)	C_v	Regime	Type
12599	OH	1.2	2.5	1.0	2.5	0.0	1.00	B	TEM
14044	OH	0.9	2.4	0.8	2.0	0.0	1.00	B	TEM
14044	L	3.0	7.9	0.8	2.0	1.8	0.60	P	η_i mode
14703	L	3.5	7.6	0.8	1.8	3.5	0.60	P	ITG
17389	L	2.0	4.9	1.1	2.0	1.8	0.60	B	TEM
17389	L	3.0	5.3	1.1	2.0	3.2	0.60	B	TEM
17389	H	3.8	8.8	1.1	2.0	6.3	0.60	B	TEM
17389	H	4.8	7.2	1.1	2.0	9.5	0.50	B	TEM
17390	L	3.0	7.7	1.1	2.0	3.2	0.60	B/P	ITG
17390	L	3.9	7.5	1.1	2.0	6.3	0.60	B	TEM/ITG
17390	H	4.7	9.1	1.1	2.0	9.5	0.50	B	TEM
17387	L	2.7	5.0	0.8	1.5	1.8	0.60	B	TEM
17387	H	3.6	7.0	0.8	1.5	3.2	0.60	B	TEM/ITG
17387	H	4.4	6.5	0.8	1.5	6.3	0.60	B	TEM
17387	H	5.0	6.5	0.8	1.5	9.5	0.50	B	TEM/ITG

Table 3. Parameters of deuterium discharges in DIII-D, JET and ASDEX analysed by transport simulations and included into the dataset VIND1.dat.

Device	Shot No	Mode	Time (s)	$\bar{n}_e$ $(10^{19}\,\mathrm{m}^{-3})$	I_p (MA)	B_t (T)	P_{inj} (MW)	C_v	Re-gime
DIII-D	82188	H	3.8	6.5	1.3	1.6	3.9	0.40	B
DIII-D	82205	H	3.7	5.3	1.3	1.9	5.8	0.35	B
JET	35156	H	55.9	5.6	2.1	2.2	8.6	0.32	B
JET	33140	H	56.5	3.7	1.6	1.8	5.8	0.25	B
JET	34340	H	56.4	5.6	2.0	2.2	17.5	0.28	B
JET	38285	H	57.4	6.6	2.6	2.6	11.4	0.20	B
JET	38415	H	56.6	4.1	1.7	1.8	15.6	0.20	B
JET	37728	H	56.6	3.1	2.6	2.7	6.5	0.30	B
ASDEX	31148	OH	1.1	2.8	0.4	2.4	0.0	1.00	B
ASDEX	31148	H	1.4	4.3	0.4	2.4	2.5	0.30	B
ASDEX	31151	OH	1.1	2.7	0.4	2.2	0.0	1.00	B
ASDEX	31151	H	1.4	4.5	0.4	2.2	2.6	0.35	B

Electron density and electron temperature profiles measured by Thomson scattering (LIDAR Thomson scattering in the case of JET) are important experimental inputs for the study. The transport model of section 2 is applied to evaluate the factor C_v in equation (4). The C_v value is varied until the measured electron density profile is recovered. A typical absolute error in determining C_v is ± 0.1. The simulated profiles of the electron density and electron temperature of all ASDEX Upgrade discharges, given in tables 1 and 2, and of the DIII-D, JET and ASDEX discharges, given in table 3, agree well with the measured profiles. The computed n_e and T_e profiles fit well at all radii within the experimental error. This means that the C_v value was chosen correctly and that the simulated L_{T_e} profiles agree with the experimental ones. In addition, the computed thermal energy content and radiative loss power inside the separatrix are in good agreement with the MHD and diamagnetic measurements and the bolometer measurements, respectively. A number of discharges from tables 1 to 3 were already simulated and discussed in [2]. The good agreement of computed and measured n_e and T_e profiles and the impact of particle sources on the density profile were documented in [2].

In all simulations, the Ware pinch is included and found to be negligibly small compared to the anomalous particle pinch, except in the central plasma region [2]. One can see from table 1 that the C_v values in deuterium discharges with predominant beam heating ($P_{inj} \geq 2.5$ MW) range from 0.2 to 0.3. They are found to be associated with large L_{T_e} values. In comparison, in Ohmic plasmas the C_v values of 1.0 and 1.1 are about four times higher and the L_{T_e} values about half as large. The high v_{in}/D ratios in the core of Ohmic discharges are responsible for the peaked density profiles measured. In the two shots with low injection heating of 1.4 MW, central OH and more peripheral NBI heating are superposed, resulting in L_{T_e} values between the Ohmic and beam-heated cases and in $C_v = 0.5$. From table 2 one can see that the C_v values in Ohmic hydrogen plasmas are close to those in Ohmic deuterium plasmas. As the temperature gradient lengths are also the same, we infer that in Ohmic plasmas C_v and $\rho_s\, v_{in}/D$

do not depend on the hydrogenic atomic mass number. In beam-heated hydrogen discharges, C_v values of 0.5 and 0.6 are found which clearly exceed those in deuterium. The corresponding L_{T_e} values are smaller than in deuterium because of the more central electron beam heating due to lower electron temperatures. It is seen from table 3 that the C_v values obtained in Ohmic and beam-heated deuterium plasmas in DIII-D, JET and ASDEX do not differ much from those in ASDEX Upgrade deuterium discharges. We conclude that high C_v values correspond to small L_{T_e} values and vice versa. Apart from this L_{T_e} dependence, C_v and $\rho_s\, v_{in}/D$ are found to be rather insensitive to the other parameters in tables 1 to 3 which exhibit large variations.

Turbulence theory predicts an anomalous transport which is specific to the collisionality regime, dominant instability and prevailing turbulence type. This important issue can be checked experimentally by studying the discharges in tables 1 to 2. The electron collisionality parameter ν_{e*} (in the range $0.46 \leq x \leq 0.68$) and the quantities R/L_{n_e}, R/L_{T_i} and $\eta_i = L_{n_i}/L_{T_i}$, evaluated at the average radius $\bar{x} = \bar{\rho}/\rho_w = 0.57$, serve to distinguish between three types of dominant turbulence: The TEM (trapped electron mode) turbulence for $\nu_{e*} < 1$ and $R/L_{n_e} \geq 3.5$, the ITG (ion temperature gradient) turbulence for $R/L_{T_i} \geq 6.0$ and $R/L_{n_e} < 3.0$, see [15], and the η_i mode turbulence for $\nu_{e*} > 1$ and $\eta_i \approx 2$. According to tables 1 and 2, the C_v (and $\rho_s v_{in}/D$) values from transport analysis do not respond to a change in the collisionality regime and are not clearly related to the prevailing turbulence type.

4. Scaling of anomalous particle pinch with dimensionless parameters and other quantities

In this section, a power-law scaling for C_v and additive two-term scalings for C_v and $\rho_s v_{in}/D$ are developed by means of multiple regression.

4.1. Representation of C_v by dimensionless parameters

It was found that the anomalous particle pinch in the confinement zone is well modeled by equation (4) with the C_v values given in tables 1 to 3. Writing equation (4) in dimensionless form leads to

$$\rho_s \frac{v_{in}(x)}{D(x)} = 2C_v \frac{x}{x_s} \qquad (6)$$

The factor C_v is expressed by the linear power-law ansatz, such as

$$C_{v,pl} = C(x)\rho_{pe*}(x)^{y_1}\nu_{e*}(x)^{y_2}\beta_{pe}(x)^{y_3}q(x)^{y_4}L_{T_e*}(x)^{y_5} \qquad (7)$$

with a dimensionless function $C(x)$ which makes the r.h.s. a constant with respect to x. Here, $\rho_{pe*} = 1.06\times 10^{-4} T_e^{0.5} B_p^{-1}\rho_s^{-1}$ is the poloidal electron gyroradius normalized to ρ_s (the effective separatrix radius), $\nu_{e*} = 1.73\times 10^{-3} Z_{eff} n_e q R \varepsilon^{-1.5} T_e^{-2}$ is the electron collisionality parameter including electron-electron and electron-ion collisions, $\beta_{pe} = 4.03\times 10^{-3} n_e T_e B_p^{-2}$ is the poloidal beta of electrons and $L_{T_e*} = L_{T_e}\rho_s^{-1} \simeq T_e |dT_e/d\rho|^{-1}\rho_s^{-1}$ is the normalized electron temperature gradient length. The units are n_e in 10^{19} m^{-3}, T_e in keV, ∇T_e in keV m^{-1}, B_p in T and R and ρ_s in m. The parameter $L_q \simeq q(dq/d\rho)^{-1}$ which varies little from discharge to discharge and the parameter T_e/T_i were not included in the ansatz. Possible dependences on these parameters will be discussed later.

Writing equation (7) in logarithmic form and averaging yields

$$\ln C_{v,pl} = \langle \ln C \rangle + y_1 \langle \ln \rho_{pe*} \rangle + y_2 \langle \ln \nu_{e*} \rangle + y_3 \langle \ln \beta_{pe} \rangle + y_4 \langle \ln q \rangle + y_5 \langle \ln L_{T_e*} \rangle \tag{8}$$

The arithmetic averaging (indicated by brackets) is carried out in the range $0.46 \leq x = \rho/\rho_w \leq 0.68$ (corresponding to $0.53 \leq x' = \rho/\rho_s \leq 0.78$). As approximately linear functions of radius are found on logarithmic scale for all parameters, one obtains to quite good approximation $\langle \ln X \rangle \simeq \ln X(\bar{x})$, where $\bar{x} = 0.57$ is the average radius (corresponding to $\bar{x}' = 0.65$). In the regression analysis, $\ln C_{v,pl}$ is the response variable, the quantities $\langle \ln X \rangle$ are the independent variables and y_1 through y_5 as well as $\langle \ln C \rangle$ are the regression parameters. For practical analysis, the statistical packages SAS and R are used [16, 17].

4.2. Statistical analysis of dataset

First, we explore the data from the deuterium and hydrogen discharges in ASDEX Upgrade, as given in tables 1 and 2. They correspond to 34 time slices (N=34). For the variables of main interest in this paper, essential statistical features of this subset of VIND1.dat are summarized in a concise form in the table 4. It presents univariate statistics, correlation coefficients (below diagonal) and partial correlation coefficients (above diagonal). The loop voltage in V is denoted by U_L. One can see from the table that, for instance, the standard deviation of $\nu_{e*}(\bar{x})$ exceeds that of $L_{T_e*}(\bar{x})$ by a factor of about five, whereas the standard deviation of $\beta_{pe}(\bar{x})$ is three times larger than that of $\rho_{pe*}(\bar{x})$. In this dataset, the $q(\bar{x})$ values range between 1.40 and 2.25. The skewness (which measures deviations from symmetry in the data) and the kurtosis (which measures both the thickness of the tail and the peakedness of the distribution) are also given [18, 19]. The table shows that the distribution of $\nu_{e*}(\bar{x})$ is not symmetric but skewed to the right. The second part of table 4 displays both correlation coefficients and partial correlations. The standard error of a correlation coefficient r is estimated by $\mathrm{SD}\,(r) = 1/\sqrt{N-1}$ which is 0.17 for N=34. For instance, according to table 4, the correlation between C_v and $L_{T_e*}(\bar{x})$ is statistically significant, since their correlation coefficient of -0.93 differs by more than two standard errors from zero. The entry (i, j) of the partial correlation matrix gives the partial correlation between variables X_i and X_j, i.e. their correlation when the influence of all other variables is 'partialled out' [18, 20]. To estimate the sample inaccuracy of the partial correlation coefficients, we use the Z-transformation to improve upon the normality of their distribution under the null-hypothesis of zero partial correlation coefficients. The standard deviation of the transformed value $Z = 0.5 \ln\,[(1+R)/(1-R)]$ of the partial correlation coefficient R equals $1/\sqrt{N-d-3}$ where d is the number of fixed covariates, see [18, 19]. Setting N=34 and $d = 5$ results in a standard error for partial correlations of approximately 0.19. The standard errors corresponding to 2 and 3 standard deviations are 0.37 and 0.53, respectively.

The partial correlation coefficients were calculated as $\left(C^{-1}\right)_{ij} / \left[\left(C^{-1}\right)_{ii} \left(C^{-1}\right)_{jj}\right]^{1/2}$ with C the correlation matrix, see [21]. It is noted that $\left(C^{-1}\right)_{ii}$ (being 16.84 for C_v) equals $\left(1 - \bar{R}^2_{m,i}\right)^{-1}$, where $\bar{R}_{m,i}$ is the well-known multiple correlation coefficient between the variable X_i and all other variables after standardisation to mean zero, see also [21]. One can directly derive that $\left(C^{-1}\right)_{ii} = (N-p-1)^{-1} \mathrm{CSS_i}/\mathrm{rmse}_i^2$, see [18], where CSS_i is the sum-of-squares of variable X_i (corrected for the mean) and $\mathrm{rmse_i}$ is the root-mean-squared error of a log-linear regression of X_i against all $p = 6$ other variables. Specifically, for the variable C_v: $\left(C^{-1}\right)_{11} = 16.84$, which is compatible with $(N-p-1)^{-1} CSS \simeq 0.37$ and $\mathrm{rmse}_1 = 14.8\,\%$.

Table 4. Univariate statistics, correlation matrix (below diagonal) and partial correlation matrix (above diagonal) for natural logarithms of variables in ASDEX Upgrade discharges (N=34). Here, $\bar{x} = \bar{\rho}/\rho_w = 0.57$ is the average radius and U_L is the loop voltage in V.

U n i v a r i a t e   S t a t i s t i c s

Variable	Mean	Std Dev	Skewness	Kurtosis	Minimum	Maximum
C_v	-0.78	0.55	0.02	-1.28	-1.61	0.10
$L_{T_e*}(\bar{x})$	-1.06	0.21	-0.31	-0.43	-1.49	-0.75
$\rho_{pe*}(\bar{x})$	-7.63	0.28	0.00	-1.29	-8.05	-7.20
$\nu_{e*}(\bar{x})$	-0.79	0.93	0.98	1.83	-2.57	2.12
$\beta_{pe}(\bar{x})$	-1.75	0.85	-0.29	-1.07	-3.28	-0.51
$q(\bar{x})$	0.53	0.16	0.42	-1.24	0.34	0.81
U_L	-0.37	0.53	0.01	-1.31	-1.27	0.49

C o r r e l a t i o n   M a t r i x   a n d   P a r t i a l   C o r r e l a t i o n   M a t r i x*

	C_v	$L_{T_e*}(\bar{x})$	$\rho_{pe*}(\bar{x})$	$\nu_{e*}(\bar{x})$	$\beta_{pe}(\bar{x})$	$q(\bar{x})$	U_L
C_v	16.84	**-0.82**	-0.26	-0.34	0.17	0.25	0.22
$L_{T_e*}(\bar{x})$	**-0.93**	1.00	-0.30	**-0.69**	**0.58**	**0.61**	0.49
$\rho_{pe*}(\bar{x})$	**-0.80**	**0.68**	1.00	-0.20	0.17	0.28	-0.34
$\nu_{e*}(\bar{x})$	0.42	-0.47	**-0.59**	1.00	**0.91**	**0.93**	**0.82**
$\beta_{pe}(\bar{x})$	**-0.85**	**0.74**	**0.89**	-0.37	1.00	**-0.85**	**-0.82**
$q(\bar{x})$	-0.20	0.13	0.14	0.49	0.12	1.00	**-0.70**
U_L	**0.81**	**-0.71**	**-0.97**	**0.65**	**-0.90**	-0.07	1.00

* Estimated (partial) correlations differing at least by two standard errors from zero are typed in italic, those differing at least by three standard errors are typed in boldface.

The constant absolute error in determining C_v is taken into account by weighted regression [16, 17]. Applying univariate regression to the subset of VIND1.dat (N=34), which comprises data from the ASDEX Upgrade discharges in tables 1 and 2, results in $C_{v,u} = 0.049\, L_{T_e*}(\bar{x})^{-2.20\pm0.13}$ with an rmse value of 21.3 %. Here, one standard deviation of the exponent equals 0.13. The C_v values from transport analysis are plotted against $L_{T_e*}(\bar{x})$ in figure 1. As discussed in section 3, three groups of data can be clearly discerned. These correspond to beam-heated deuterium plasmas (low C_v and large L_{T_e*}), beam-heated hydrogen plasmas (medium C_v and medium L_{T_e*}) and Ohmic plasmas in deuterium and hydrogen (high C_v and small L_{T_e*}), respectively. The straight line represents the $L_{T_e*}(\bar{x})$ dependence of the univariate scaling. Note that the univariate result is to be interpreted as the dependence of $C_{v,u}$ on $L_{T_e*}(\bar{x})$ when the other parameters 'covary' with $L_{T_e*}(\bar{x})$ according to table 4.

Applying weighted multiple log-linear regression to the subset of VIND1.dat (N=34, ASDEX Upgrade discharges in tables 1 and 2) yields the following trivariate power-law scaling

$$C_{v,pl} = 0.065\, L_{T_e*}(\bar{x})^{-1.92\pm0.17} U_L^{0.42\pm0.08} \nu_{e*}(\bar{x})^{-0.11\pm0.03} \tag{9}$$

with an rmse value of 14.9 %. The same weighting was performed as for the scaling relation given in equation (10). It is obvious from equation (9) that the electron temperature gradient length is the strongest parameter with an exponent equal to 11.3 times its standard deviation 0.17. The exponent of $L_{T_e*}(\bar{x})$ is statistically highly significant. We thus conclude that the electron temperature gradient length is the key parameter of the anomalous particle pinch, in agreement with [2]. The influence of a large number of further quantities was tested by regression analysis. It is found that the loop voltage is an additional parameter of influence which introduces $\nu_{e*}(\bar{x})$. Equation (9) shows that the exponents of U_L and $\nu_{e*}(\bar{x})$ are both statistically significant. The loop voltages taken from the simulations are compatible with measured U_L values. In the trivariate scaling of equation (9), the meaning of the $L_{T_e}^{-1.92}$ dependence is that it holds at constant U_L and $\nu_{e*}(\bar{x})$. The 'statistical relevance' [22] for predicting C_v is defined as the absolute value of the exponent of a regression variable times the standard deviation of this variable, see table 4. For the parameters L_{T_e*}, U_L and ν_{e*} one obtains 0.40, 0.22 and 0.10, respectively. Omitting the six Ohmic discharges in the regression analysis is found to deteriorate somewhat the conditioning while a sensible regression is still possible. For the L- and H-mode discharges in deuterium and hydrogen, the power-law scaling is essentially the same as in equation (9).

When performing 4-variate regression by using $\rho_{pe*}(\bar{x})$, $\beta_{pe}(\bar{x})$ or $q(\bar{x})$ in addition to the variables in equation (9), the exponents of $\rho_{pe*}(\bar{x})$, $\beta_{pe}(\bar{x})$ and $q(\bar{x})$ were found to be not statistically significant. It is stressed that this is also true for $\nu_{e*}(\bar{x})$, as long as a loop voltage dependence is not introduced. In the dataset, the parameter ν_{e*} varies by more than two and a half orders of magnitude. Furthermore, the residuals $\ln\left(C_v/C_{v,pl}\right)$ were plotted against the logarithms of the variables $\rho_{pe*}(\bar{x})$, $\beta_{pe}(\bar{x})$ and $q(\bar{x})$ to check for the absence of outliers and quadratic dependences. Note that the rmse value of 14.9 % of the power-law scaling is considerably lower than the rmse value of 21.3 % of the univariate scaling. This indicates the improvement achieved by including the loop voltage. In addition, univariate regression with L_q and bivariate regression with L_{T_e} and L_q did show that, within the class of simple power laws considered here, C_v does not depend significantly on L_q. This does not support an expression like $v_{in}/D \propto L_q^{-1} \propto \nabla q/q$ (curvature pinch), reported in [23]. Furthermore, C_v does not depend significantly on T_e/T_i either.

Substituting C_v in equation (4) with the scaling in equation (9) leads to $n_e v_{in} \propto n_e D(\nabla T_e/T_e)^2$, i.e. the anomalous inward flux is driven by the square of the electron temperature gradient. This process causes the main contribution to the anomalous inward flux. It is connected with the terms $\tilde{\mathbf{v}}_E{\cdot}\nabla T_e$ and $\tilde{\mathbf{v}}_E{\cdot}\nabla \tilde{T}_e$, i.e. with perpendicular dynamics of turbulence. Here, $\tilde{\mathbf{v}}_E$ is the fluctuating $\mathbf{E} \times \mathbf{B}$ drift velocity and $\tilde{T}_e$ is the electron temperature fluctuation.

In addition, the dependence of C_v on the loop voltage suggests a further off-diagonal term in the transport matrix equation due to the Ohmic inductive electric field $E_{\|}$ which is connected with parallel dynamics of turbulence. As mentioned above, transport analysis is carried out during the flat-top phase of the current. Our simulations show that $E_{\|}$ is radially independent and given by $U_L/(2\pi R)$, because resistive equilibrium has been reached. Quasilinear models for anomalous inward fluxes driven by fluctuations and the Ohmic inductive electric field predict $C_{v,ql} \propto E_{\|}/\nu_e$ in the plateau regime [24] and $C_{v,ql} \propto E_{\|}/\nu_e^{0.5}$ in the banana regime [25] where ν_e is the electron collision frequency including electron-electron and electron-ion collisions. Thus, for this particle pinch contribution collisions are crucial. The combined appearance of loop voltage and collisionality in equation (9) supports this mechanism. A coupling of the L_{T_e} and $E_{\|}$ components in the experiment is thought to be unlikely, because they are based on perpendicular and parallel dynamics, respectively, with quite different time scales. A characteristic frequency of parallel electron dynamics is the electron transit frequency $\omega_{te} = k_{\|}v_e$ which is much higher than the electron drift frequency ω_{*e} characterizing perpendicular electron dynamics. Here, $k_{\|} \simeq (qR)^{-1}$ is the parallel wave number and v_e is the electron thermal velocity. Thus, turbulence theory suggests that the L_{T_e} and $E_{\|}$ components of the anomalous particle pinch are not coupled and should be modeled as two separate terms.

In this context, tokamak experiments with non-inductive current drive and zero loop voltage are interesting, since $E_{\|} = 0$ does not only mean vanishing Ware pinch but also vanishing $E_{\|}$ component of the anomalous particle pinch. The evidence of an anomalous particle pinch in the case of $E_{\|} = 0$ in experiments with lower hybrid current drive (LHCD) in Tore Supra [26] and electron cyclotron current drive (ECCD) in TCV [27] corroborates an ansatz separating the L_{T_e} and $E_{\|}$ terms. Moreover, nonzero C_v values for $U_L = 0$ rule out simple power laws like that in equation (9).

For fitting an additive two-term model, we first applied unweighted least squares regression to the ASDEX Upgrade subset of VIND1.dat (N=34) with PROC NLIN from the package SAS [16]. Using the SAS results as starting values, we applied in a second step a weighted (generalised) nonlinear least squares analysis, while assuming a constant error on C_v, i.e. the variance of $\ln C_v$ being proportional to C_v^{-2}. This was carried out with the program nlme [17] of the public-domain statistical package R. The result of this approach is the two-term scaling

$$C_{v,tt} = 0.0216\, L_{T_e*}(\bar{x})^{-2.58\pm0.38} + 0.154\, U_L^{1.55\pm0.61} \nu_{e*}(\bar{x})^{-0.42\pm0.21} \tag{10}$$

with an rmse value of 15.2 %. The scaling is based on the deuterium and hydrogen discharges in ASDEX Upgrade, given in tables 1 and 2. The numerical constants in both terms apply for L_{T_e*} and ν_{e*} taken at the average radius $\bar{x} = \bar{\rho}/\rho_w = 0.57$. The constant in the second term is dimensional in contrast to the constant in the first term. Equation (10) shows that the electron temperature gradient length is the strongest parameter with an exponent equal to 6.8 times its standard deviation of 0.38 which is statistically highly significant. As can be seen, the exponents of U_L and $\nu_{e*}(\bar{x})$ in the second term are both statistically significant. Note that the loop voltage introduces the ν_{e*} dependence, i.e. U_L and ν_{e*} form a pair of parameters. It should be mentioned that the two-term scaling in equation (10) is similar to an offset nonlinear scaling [28]. The values for the 'statistical relevance' of L_{T_e*}, U_L and ν_{e*} are approximately the same as those of the power-law scaling $C_{v,pl}$, if a 20 % contribution to $C_{v,tt}$ due to the second term in equation (10) is taken into account (see below).

In figure 2, $C_{v,tt} - C_{v,U}$ is plotted against $L_{T_e*}(\bar{x})$, where $C_{v,U}$ is the second term in equation (10). The straight line gives the dependence of the first term on $L_{T_e*}(\bar{x})$. It is further found univariately that $C_{v,tt} - C_{v,U}$ does not depend significantly on ρ_{pe*}, β_{pe} and ν_{e*}. Figure 3 shows a clear correlation of the loop voltage U_L with the electron collisionality parameter $\nu_{e*}(\bar{x})$ but not a strong collinearity, which enables an efficient simultaneous estimation of the exponents in the term $C_{v,U}$. The variables U_L and $\nu_{e*}(\bar{x})$ appear as a pair in the regression analysis. A plot of the C_v values from transport analysis against the $C_{v,tt}$ values predicted by equation (10) is presented in figure 4. As can be seen, the two-term scaling yields a reasonably tight fit (rmse value of 15.2 %) in view of the error in determining the C_v values by transport analysis.

Applying equation (10) to the ASDEX Upgrade discharges in tables 1 and 2 shows that for high heating power ($P_{inj} \geq 4.8\,\mathrm{MW}$) the average contribution of the second term $C_{v,U}$ to $C_{v,tt}$ is some 20 %. In the case of NB heated discharges with lower heating power, $C_{v,U}$ contributes on the average by 35 %. Thus, the L_{T_e} term is dominant, but the $E_\|$ contribution must not be neglected. According to table 4, both U_L and $\nu_{e*}(\bar{x})$ are correlated with $L_{T_e*}(\bar{x})$, so that they introduce an implicit L_{T_e} dependence into $C_{v,tt}$. In equation (10), the effective exponent of L_{T_e*} varies with the magnitude of the second term. At the average radius $\bar{x}$, the exponent equals -2.58 for vanishing $C_{v,U}$ and 0 for vanishing first term. For the $C_{v,U}$ values of the discharges in tables 1 and 2, one calculates effective L_{T_e*} exponents in the range -1.4 to -2.4. The exponent -1.92 in the power-law scaling of equation (9) lies close to the middle of this interval.

Transport modellings can be carried out with the two-term scaling $C_{v,tt}$ of equation (10) substituted in equation (4) which provides the anomalous particle pinch in the confinement zone. To facilitate the use of this scaling in modellings that do not include the SOL, we introduce $x' = \rho/\rho_s$ with the corresponding average value $\bar{x}' = 0.65$. Combining equations (6) and (10) then leads to the following two-term scaling law

$$\rho_s \frac{v_{in}(x')}{D(x')} = 0.0432 \left[\left(\frac{L_{T_e}(\bar{x}')}{\rho_s} \right)^{-2.58} + 7.13\, U_L^{1.55} \nu_{e*}(\bar{x}')^{-0.42} \right] x' \qquad (11)$$

A formulation with $L_{T_e*}(x')$ and $\nu_{e*}(x')$ requires radially dependent factors $f(x')$ and $g(x')$ in the first and second term, respectively, (see the factor $C(x)$ in equation (7)) which make $C_{v,tt}$ radially independent. Applying $L_{T_e}(\bar{x}') = L_{T_e}(x')f(\bar{x}')/f(x')$ and $\nu_{e*}(\bar{x}') = \nu_{e*}(x')g(\bar{x}')/g(x')$ in equation (11) yields the scaling expression

$$\rho_s \frac{v_{in}(x')}{D(x')} = 0.0795 \left[f(x')^{2.58} \left(\frac{L_{T_e}(x')}{\rho_s} \right)^{-2.58} + 7.19\, U_L^{1.55} g(x')^{0.42} \nu_{e*}(x')^{-0.42} \right] x' \qquad (12)$$

with $f(x') = 1 - 0.02x' - 0.34x'^2$ and $g(x') = 1 - 3.17x' + 2.85x'^2$. The L_{T_e} and ν_{e*} profiles in VIND1.dat are used to determine $f(x')$ and $g(x')$. Simulations have shown that the scaling in equation (12) can replace equation (4) and the strongly rising v_{in}/D profile near the edge, i.e. it works both in the confinement zone and in the edge region.

Comparison with theory is facilitated, if we replace U_L and ν_{e*} with the parameters $E_\|$ and ν_e. Applying weighted regression to the subset of VIND1.dat (N=34) results in the scaling

$$C_{v,tt1} = 0.0267\, L_{T_e*}(\bar{x})^{-2.44\pm0.30} + 1.13 \times 10^5\, E_\|^{1.73\pm0.68} \nu_e(\bar{x})^{-0.75\pm0.35} \qquad (13)$$

with an rmse value of 15.2 %. This scaling fits the data as well as that in equation (10). Writing the second term as $1.13\times10^5\left(E_{\|}/\nu_e(\bar{x})^{0.43}\right)^{1.73}$ reveals that the expression in brackets is close to the quasilinear prediction $C_{v,ql} \propto E_{\|}/\nu_e^{0.5}$ for the banana regime [25]. This comparison is appropriate, since 80 % of the plasmas simulated are in the banana regime (see tables 1 and 2). The novel enhanced particle pinch is attributed to a linear term, $-(e/m_e)E_{\|}\partial\tilde{f}_e/\partial v_{\|}$, in the drift kinetic equation where $\tilde{f}_e$ is the fluctuating electron distribution function and $v_{\|}$ is the particle velocity parallel to $\mathbf{B}$.

Many quasilinear fluid and kinetic models, see [2], predict the linear scaling $v_{in}/D \propto L_{T_e}^{-1}$, i.e. $C_v \propto \rho_s v_{in}/D \propto (L_{T_e}/\rho_s)^{-1}$. It is interesting that equations (9) to (12) indeed recover a dependence on the inverse of the parameter $L_{T_e}/\rho_s = L_{T_e *}$, but disprove the linearity of the scaling predicted. The ∇T_e driven anomalous particle pinch term in equations (10) to (12) was found to scale strongly nonlinearly with $L_{T_e *}$. In our analysis, a novel anomalous particle pinch term driven by $E_{\|}$, for which collisions are crucial, was experimentally revealed. Here, again a dependence on the factor $E_{\|}/\nu_e^{0.5}$, predicted by quasilinear theory, was recovered, while the linearity of the scaling was otherwise disproved. It is thus concluded that quasilinear theory helped to identify two driving processes of the anomalous particle pinch. On the other hand, the nonlinear scalings in equations (10) to (12) show that quasilinear theory is ruled out by experiment.

The univariate scaling $C_{v,u} = 0.049\,(L_{T_e}(\bar{x}')/\rho_s)^{-2.20}$ is relevant for comparison with the semi-empirical expressions from transport analysis and simulations in [2]

$$C_{v,se} = \frac{1}{2}C_t\frac{1}{x'^2}\left(\frac{L_{T_e}(x')}{\rho_s}\right)^{-2} \tag{14}$$

and

$$\rho_s\frac{v_{in}(x')}{D(x')} = C_t\frac{1}{x'}\left(\frac{L_{T_e}(x')}{\rho_s}\right)^{-2} \tag{15}$$

with $C_t = 3.47\times10^{-2}$. It is obvious that the univariate regression almost recovers the previous semi-empirical results. In [2], equation (15) was shown to work both in the core and in the edge region.

Some quasilinear models invoke a scaling $v_{in}/D \propto \left(c_T L_{T_e}^{-1} + c_q L_q^{-1}\right)$ which was, for instance, applied in studies in [29]. As discussed above for equations (9) to (11), the linear $L_{T_e}^{-1}$ scaling is disproved by experiment. Based on the ASDEX Upgrade subset (N=34), we fit the linear combination of $L_{T_e}^{-1}$ and L_q^{-1} to some power and obtain $C_v = 0.06\left[(1.3\pm0.4)L_{T_e}(\bar{x})^{-1} - (0.5\pm0.4)L_q(\bar{x})^{-1}\right]^{1.6\pm0.35}$. The corresponding rmse value of 19.0 % is better than the rmse value of 21.3 % of the univariate scaling but notably worse than the rmse value of 15.2 % of the two-term scaling in equation (10). Note that an inward directed curvature pinch ($c_q > 0$), as predicted by theory, would require an exponent of at least 2.5 (instead of 1.6) which is outside the statistical error bar. We find that a linear ansatz is incompatible with a positive curvature pinch term.

The dependence of C_v on the plasma size is crucial for the extrapolation to reactor-grade devices. Therefore, one main objective of including DIII-D, JET and ASDEX discharges in VIND1.dat was to alter the machine size. In the shots of table 3, the effective separatrix radius

ρ_s varies by a factor of 3. As this parameter occurs in $L_{T_e*} = L_{T_e}/\rho_s$, the two-term scaling $C_{v,tt}$ in equation (10) already includes a dependence on the plasma size. In figure 5, the C_v values from transport analysis of all ASDEX Upgrade, DIII-D, JET and ASDEX discharges in tables 1 to 3 are plotted against the $C_{v,tt}$ values predicted by equation (10). As can be seen, the two-term scaling $C_{v,tt}$ based on ASDEX Upgrade data predicts rather well also the other tokamaks with different machine size (denoted by open symbols) which is attributed to the $L_{T_e*} = L_{T_e}/\rho_s$ dependence in equation (10).

Applying weighted multiple regression to the whole dataset VIND1.dat (N=46), comprising the 46 time slices of the ASDEX Upgrade, DIII-D, JET and ASDEX discharges in tables 1 to 3, results in the scaling

$$C_{v,tt2} = 0.0219\, L_{T_e*}(\bar{x})^{-2.54\pm0.41} + 992.3\, U_L^{1.34\pm0.43} \nu_e(\bar{x})^{-0.67\pm0.27} \qquad (16)$$

with an rmse value of 18.1 %. Here, the scaling with the electron collision frequency ν_e is given, because it yields a slightly smaller rmse value than ν_{e*}. In figure 6, a plot of the C_v values from transport analysis against the $C_{v,tt2}$ values is presented which shows that the scaling in equation (16) yields a rather good fit for all tokamaks with varying size. The L_{T_e*} dependence of $C_{v,tt2}$ agrees with that in equation (10). It is concluded that the $L_{T_e*} = L_{T_e}/\rho_s$ scaling covers the dependence of C_v and $\rho_s\, v_{in}/D$ on the effective plasma radius. Thus, the $C_{v,tt}$ and $\rho_s\, v_{in}/D$ scalings in equations (10) to (12) can be used to predict the anomalous particle pinch in devices with varying size and have a predictive potential for ITER.

Transport simulations of an ITER inductive scenario with $Q = P_{fus}/P_{inj} = 10$ and fusion power $P_{fus} = 400\, MW$ have shown that the central heating due to alpha particles causes narrower temperature profiles. Compared with ASDEX Upgrade, one obtains 1.5 times smaller $L_{T_e*} = L_{T_e}/\rho_s$ values and a 2.8 times higher L_{T_e*} term in the $C_{v,tt}$ scaling in equation (10). The scaling predicts C_v values near 0.7, high values of $\rho_s v_{in}/D$ and rather peaked density profiles in ITER. Here, the anomalous particle pinch is due to the L_{T_e} term, whereas the contribution of the $E_\parallel$ driven term is negligibly small. These results are confirmed by simulations of the ITER inductive scenario with the scaling of equation (12) used both in the core and in the edge region. The simulations, conducted with the recently developed χ scaling [7] and $\chi_e/\chi = 2/3$, $D/\chi_e = 0.9$ and $\chi_i/\chi_e = 2$, predict rather peaked profiles of electron, deuteron and triton densities for gas-puffed scenarios. The density peaking is found to improve the calculated energy confinement time by 18 % relative to a case with flat density profiles, simulated with $v_{in} = 0$. More recent nonlinear τ_E scalings [1, 30] indicate a point prediction for ITER close to 0.85 times the value predicted by ITERH-98P(y, 2). Keeping P_{fus} at 400 MW, this corresponds to Q values near 5 (rather than 10) for which one expects larger L_{T_e*} and smaller C_v values.

In addition to the analysis above, the effect of L_{T_e} on the anomalous particle pinch is explored by studying an Ohmic discharge in JET with current ramp-up (No 19649) which exhibits a flat electron density profile. Transport analysis resulted in $C_v \simeq 0.3$ only which is small compared with the $C_v \simeq 1.0$ values during current flat top in tables 1 and 2. Simulations showed that during current ramp-up the current density profile is considerably broader (corresponding to a 40 % decline of the internal inductance) and the Ohmic heating power is strongly reduced in the central plasma. As a consequence, the measured and computed L_{T_e} values are 1.5 times larger than in the case of constant plasma current. The L_{T_e} scalings in equations (10) and (16) predict a reduction of C_v from 1.0 to 0.3, in agreement with $C_v \simeq 0.3$ from transport analysis.

5. Conclusions

A detailed statistical analysis of the anomalous particle pinch through the ratio $\rho_s v_{in}/D$ was carried out by examining a large number of possible parameter dependences. A dataset covering a wide parameter range was analysed. The data from ASDEX Upgrade are well-conditioned with respect to $\bar{n}_e$, I_p, B_t and P_{inj} (see tables 1 and 2) and to the dimensionless parameters. Results from transport analysis of the discharges in tables 1 to 3, comprising profiles of $\rho_s v_{in}/D$, ρ_{pe*}, ν_{e*}, β_{pe}, q and L_{T_e*} and many further quantities in the confinement zone, were compiled in the special anomalous particle pinch dataset VIND1.dat. It is emphasized that transport analysis is necessary to determine the anomalous particle pinch and v_{in}/D from measured density profiles with sufficient accuracy and to separate the effect of particle sources on the density profile, see [2].

The anomalous particle pinch in a set of Ohmic, L- and H-mode deuterium and hydrogen discharges from ASDEX Upgrade, DIII-D, JET and ASDEX was evaluated by transport simulations, using a special version of the 1.5-D BALDUR transport code and applying the transport model described in section 2. It was found that the anomalous particle pinch in the confinement zone is well modeled by equation (4) with the C_v values given in tables 1 to 3. The C_v values are low in beam-heated deuterium plasmas, medium in beam-heated hydrogen plasmas and high (close to 1) in Ohmic deuterium and hydrogen plasmas. High C_v values are found to be associated with small L_{T_e} values and vice versa. Apart from that, C_v and $\rho_s v_{in}/D$ are rather insensitive to the other parameters in tables 1 to 3 which vary largely. Another important result is that, contrary to theoretical predictions, the C_v and $\rho_s v_{in}/D$ values from transport analysis do not respond to a change in collisionality regime (B, P and PS) and are not clearly related to the type of prevailing turbulence (TEM, ITG and η_i mode).

A principal subset of VIND1.dat, which comprises the data from the ASDEX Upgrade shots in tables 1 and 2 (N=34), was examined first. An essential statistical summary covering univariate statistics, correlation coefficients and partial correlation coefficients was given in table 4. Applying multiple log-linear weighted regression to this subset of VIND1.dat resulted in the power-law scaling $C_{v,pl}$ in equation (9) with an rmse value of 14.9 %. It shows that the electron temperature gradient length is the key parameter of the anomalous particle pinch and that its exponent is statistically highly significant. By contrast, the exponents of the dimensionless parameters $\rho_{pe*}(\bar{x})$, $\beta_{pe}(\bar{x})$ and $q(\bar{x})$ were found to be not statistically significant. A check of many further quantities by regression analysis revealed that the loop voltage is an additional parameter of influence which enters together with $\nu_{e*}(\bar{x})$. The exponents of U_L and $\nu_{e*}(\bar{x})$ are both statistically significant. It is stressed that $C_{v,pl}$ is independent of the electron collisionality parameter, as long as the loop voltage is not included.

The power-law scaling in equation (9) suggests that two off-diagonal terms contribute to the anomalous inward flux: One driven by the square of the electron temperature gradient and independent of the collisionality parameter and the other driven by the Ohmic inductive electric field and based on collisions. This idea is supported by quasilinear transport models for the plateau and banana regimes [24, 25]. The L_{T_e} and $E_{\|}$ terms are expected to be decoupled, since they are based on perpendicular and parallel dynamics, respectively, with quite different time scales. Moreover, the evidence of an anomalous particle pinch in non-inductive current drive experiments with zero loop voltage confirms a C_v model with separate L_{T_e} and $E_{\|}$ components and rules out the power-law scaling in equation (9).

For fitting an additive two-term model, weighted nonlinear least squares analysis was applied to the subset of VIND1.dat (N=34). It yielded the two-term scaling laws $C_{v,tt}$ and $\rho_s v_{in}/D$, given in equations (10) and (11), with an rmse value of 15.2 %. The exponent of $L_{T_e*}(\bar{x})$ is statistically highly significant and the exponents of U_L and $\nu_{e*}(\bar{x})$ are both statistically significant. It was inferred that $L_{T_e*} = L_{T_e}/\rho_s$ is the key parameter of the anomalous particle pinch in tokamaks, in agreement with [2]. The ∇T_e driven anomalous particle pinch term in equations (10) to (12) exhibits a strongly nonlinear L_{T_e*} scaling. In addition, a new anomalous particle pinch term driven by $E_{\|}$, for which collisions are important, was experimentally discovered. It is attributed to a linear term, $-(e/m_e)E_{\|}\partial\tilde{f}_e/\partial v_{\|}$, in the drift kinetic equation. Quasilinear theory was found to help identify two basic processes of the anomalous particle pinch. On the other hand, the nonlinearity of the scalings in equations (10) to (12) shows that quasilinear theory is disproved by experiment. The main contribution to $C_{v,tt}$ in equation (10) is due to the L_{T_e} term, whereas the $E_{\|}$ term contributes by about 20 %. The two-term scaling in equation (12), derived from equation (11), was successfully applied in simulations both in the core and in the edge region. It can replace equation (4) and the strongly rising v_{in}/D near the edge. Weighted univariate regression resulted in $C_{v,u} \propto L_{T_e}^{-2.20}$ which is close to the semi-empirical $C_{v,se} \propto L_{T_e}^{-2}$ scaling from transport analysis and simulations [2].

The scaling of the anomalous particle pinch with the plasma size was explored by varying the effective separatrix radius ρ_s by a factor of 3. Applying weighted multiple regression to VIND1.dat (N=46, all ASDEX Upgrade, DIII-D, JET and ASDEX discharges in tables 1 to 3) yielded the expression $C_{v,tt2}$ in equation (16). Its $L_{T_e*} = L_{T_e}/\rho_s$ scaling agrees with that of $C_{v,tt}$ in equation (10) and covers the dependence of C_v and $\rho_s v_{in}/D$ on the effective plasma radius. Thus, the scaling laws in equations (10) to (12) can be used to predict the anomalous particle pinch in devices with varying size and in ITER.

Simulations of an inductive ITER scenario with $Q = 10$ showed that the central heating due to alpha particles reduces L_{T_e}, so that the L_{T_e}/ρ_s term in equation (10) rises considerably. This term is responsible for the anomalous particle pinch in ITER, while the $E_{\|}$ driven term is negligibly small. The two-term scaling $C_{v,tt}$ predicts C_v values near 0.7 and high $\rho_s v_{in}/D$ values in ITER which correspond to rather peaked density profiles. Simulations applying the scaling of equation (12) in the core and edge regions yielded peaked density profiles and an 18 % improvement of the energy confinement time over a flat density profile case with $v_{in} = 0$.

References

[1] Mukhovatov V. *et al* 2003 *Nucl. Fusion* **43** 942

[2] Becker G. 2004 *Nucl. Fusion* **44** 933

[3] Singer C.E. *et al* 1988 *Comput. Phys. Commun.* **49** 275

[4] Becker G. 1995 *Nucl. Fusion* **35** 39

[5] Becker G. 1996 *Nucl. Fusion* **36** 527

[6] H-Mode Database Working Group (presented by Kardaun O.) 1993 *Proc. 14th Int. Conf. on Plasma Physics and Controlled Nuclear Fusion Research* (*Wuerzburg*, 1992) vol 3 (Vienna: IAEA) p 251

[7] Becker G. 2004 *Nucl. Fusion* **44** L26

[8] ITER Physics Basis 1999 *Nucl. Fusion* **39** 2175

[9] Kardaun O.J.W.F. 1999 *Plasma Phys. Control. Fusion* **41** 429
[10] Becker G. 1999 *Nucl. Fusion* **39** 95
[11] Becker G. and Murmann H. 1988 *Nucl. Fusion* **28** 2179
[12] Becker G. *et al* 1982 *Nucl. Fusion* **22** 1589
[13] Becker G. 1984 *Nucl. Fusion* **24** 1364
[14] The ITER 1D Modelling Working Group: Boucher D. *et al* 2000 *Nucl. Fusion* **40** 1955
[15] Jenko F. *et al* 2005 *Plasma Phys. Control. Fusion* **47** B195
[16] SAS Institute Inc., Cary, NC. SAS/STAT User's Guide, 1985, version 5, ISBN 0-917382-66-8, also 2000, version 8, first edition; procedures REG and NLIN
[17] The R Development Core Team, R: A language and environment for statistical computing, version 2.1.1.; procedure nlme by Pinheiro J. and Bates D., 2005
[18] Kardaun O.J.W.F., Classical methods of statistics, Springer-Verlag, Heidelberg, 2005
[19] Kendall M., Stuart A. and Ord K., The advanced theory of statistics, Griffin, London, 1987, Vol. II, fourth edition
[20] Kshirsagar A. M., Multivariate analysis. Marcel Dekker, New York, 1972
[21] Whittaker J., Graphical models in applied multivariate statistics, Wiley, New York, 1990
[22] Kardaun O., Handbook of statistics (C.R. Rao, R. Chakraborty editors), Vol. 8 (chapter 14, section 3.1.1), Elsevier, Amsterdam, 1991
[23] Baker D.R. 2002 *Phys. Plasmas* **9** 2675
[24] Shaing K.C. 1988 *Phys. Fluids* **31** 2249
[25] Shaing K.C. and Hazeltine R.D. 1990 *Phys. Fluids B* **2** 2353
[26] Hoang G.T. *et al* 2003 *Phys. Rev. Lett.* **90** 155002-1
[27] Zabolotsky A. *et al* 2003 *Plasma Phys. Control. Fusion* **45** 735
[28] Takizuka T. 1998 *Plasma Phys. Control. Fusion* **40** 851
[29] Garzotti L. *et al* 2003 *Nucl. Fusion* **43** 1829
[30] Kardaun O.J.W.F. 2002 $IPP-IR-2002/5-1.1$ *Report* Max-Planck-Institut für Plasmaphysik, Garching and http://www.ipp.mpg.de/ipp/netreports

Figure Captions

Figure 1. Log-log plot of C_v values from transport analysis at 34 time slices from deuterium and hydrogen discharges in ASDEX Upgrade, given in tables 1 and 2, against normalized electron temperature gradient length $L_{T_e*}(\bar{x}) = L_{T_e}(\bar{x})/\rho_s$ with ρ_s the effective separatrix radius and $\bar{x} = 0.57$ the average radius. The straight line shows the univariate scaling $C_{v,u} = 0.049\, L_{T_e*}(\bar{x})^{-2.20}$.

Figure 2. Log-log plot of $C_{v,tt} - C_{v,U}$ versus $L_{T_e*}(\bar{x})$, where $C_{v,U} = 0.154\, U_L^{1.55} \nu_{e*}(\bar{x})^{-0.42}$. The straight line represents the $L_{T_e*}(\bar{x})$ dependence of the first term in the two-term scaling $C_{v,tt}$ in equation (10).

Figure 3. Log-log plot of electron collisionality parameter $\nu_{e*}(\bar{x})$ versus loop voltage U_L in V. The plot shows a clear correlation but not a strong collinearity between U_L and $\nu_{e*}(\bar{x})$.

Figure 4. Log-log plot of C_v values from transport analysis of ASDEX Upgrade discharges versus $C_{v,tt}$ values predicted by the two-term scaling in equation (10).

Figure 5. Log-log plot of C_v values from transport analysis of discharges in ASDEX Upgrade (dots), DIII-D (triangles), JET (squares) and ASDEX (diamonds) versus $C_{v,tt}$ values predicted by the two-term scaling in equation (10). Although this scaling is based on ASDEX Upgrade data, it also works for the other tokamaks with different machine size.

Figure 6. Log-log plot of C_v values from transport analysis of discharges in ASDEX Upgrade (dots), DIII-D (triangles), JET (squares) and ASDEX (diamonds) versus $C_{v,tt2}$ values predicted by the two-term scaling in equation (16) based on the whole dataset VIND1.dat with 46 time slices.

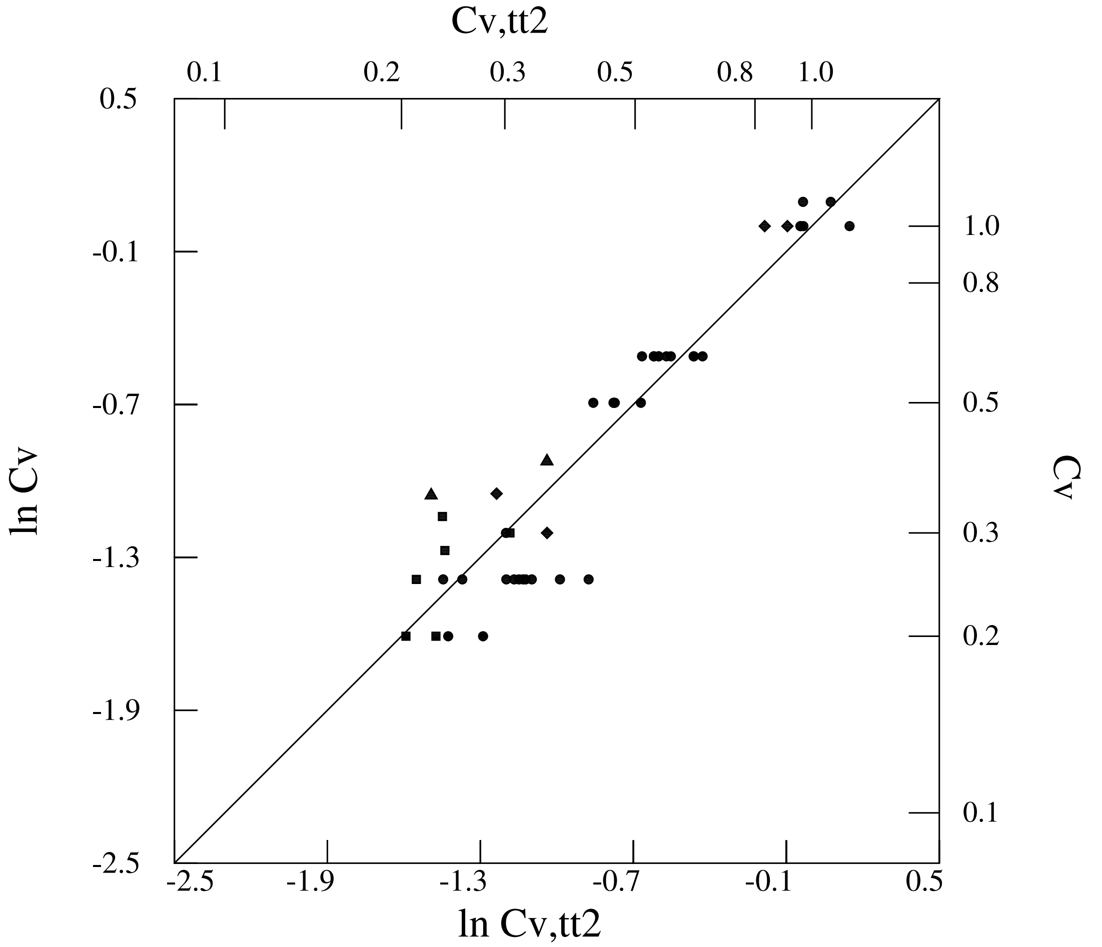

Cv,tt2
0.1
0.2
0.3
0.5
0.8
1.0
0.5
-0.1
-0.7
-1.3
-1.9
-2.5
ln Cv
1.0
0.8
0.5
0.3
0.2
0.1
Cv
-2.5
-1.9
-1.3
-0.7
-0.1
0.5
ln Cv,tt2

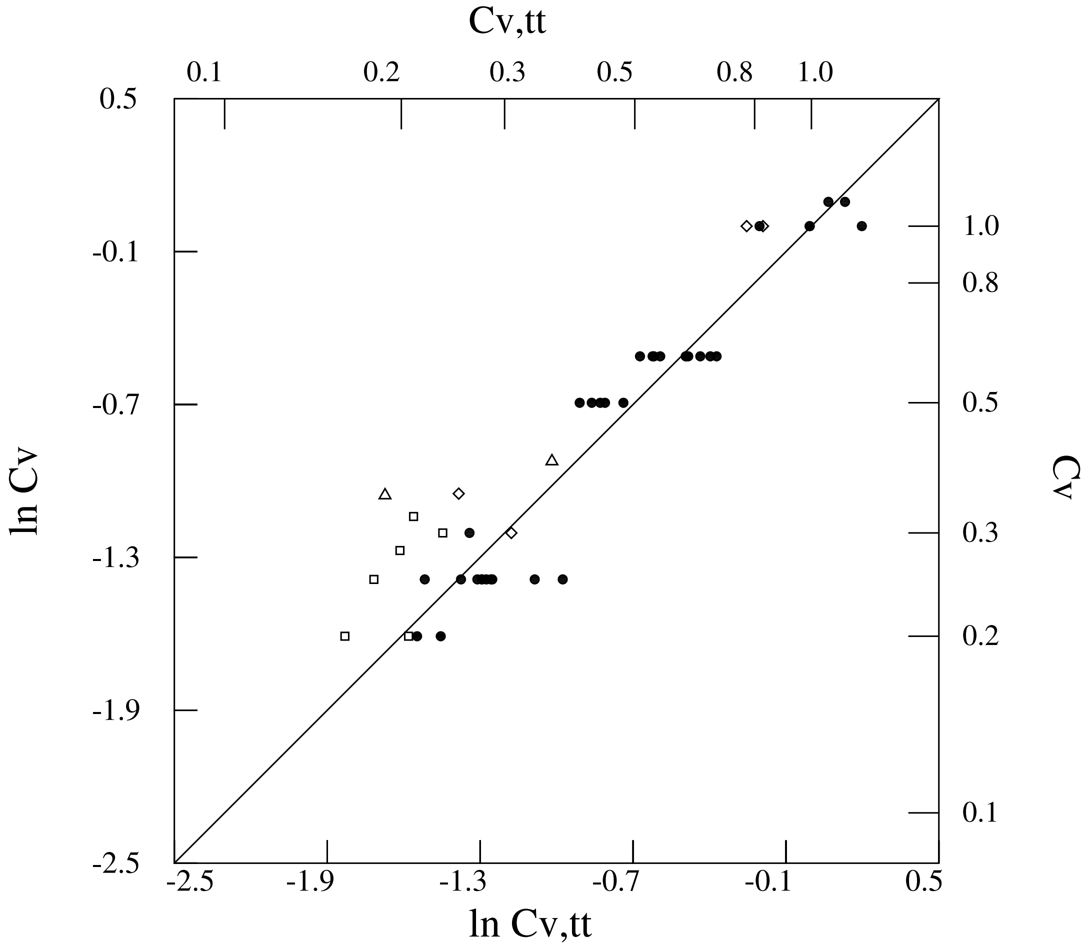

Cv,tt
0.1
0.2
0.3
0.5
0.8
1.0
0.5
-0.1
-0.7
-1.3
-1.9
-2.5
ln Cv
1.0
0.8
0.5
0.3
0.2
0.1
Cv
-2.5
-1.9
-1.3
-0.7
-0.1
0.5
ln Cv,tt

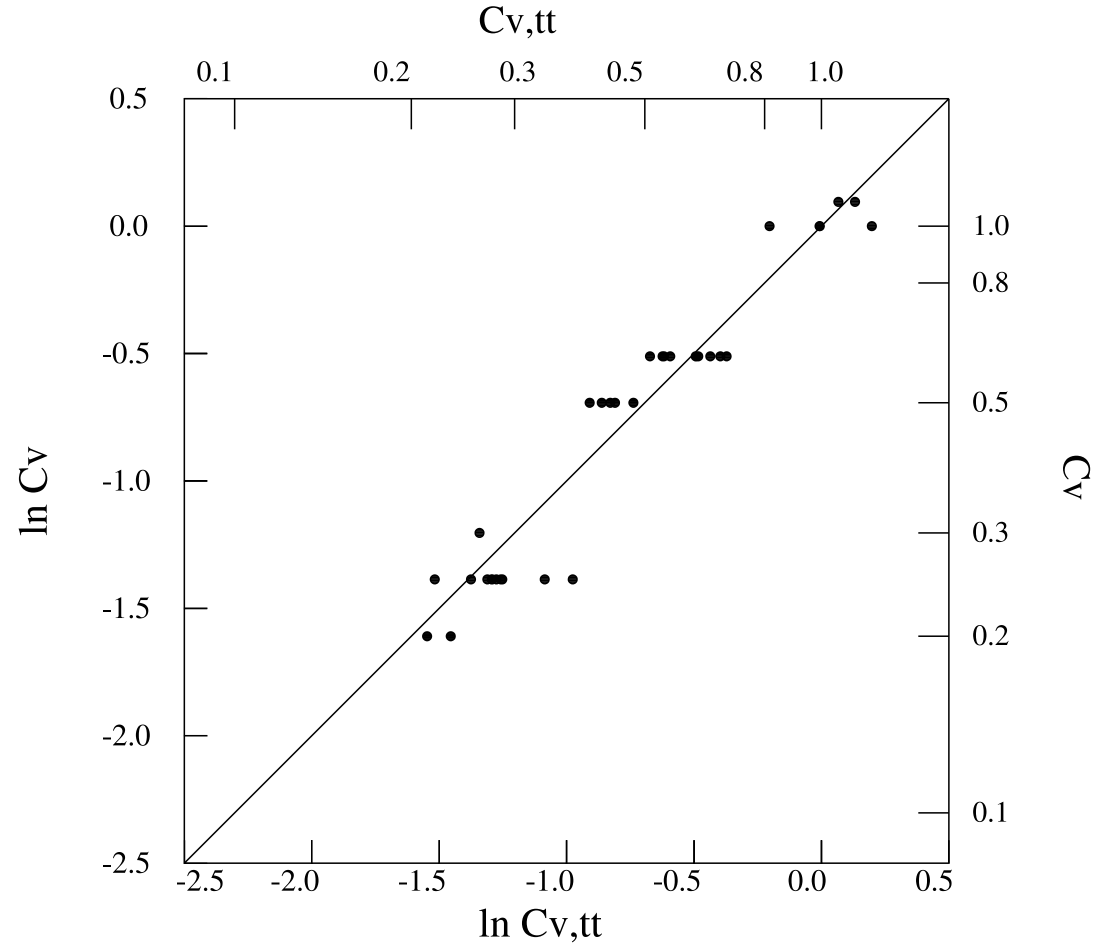

Cv,tt
0.1
0.2
0.3
0.5
0.8
1.0
0.5
0.0
-0.5
-1.0
-1.5
-2.0
-2.5
ln Cv
1.0
0.8
0.5
0.3
0.2
0.1
Cv
-2.5
-2.0
-1.5
-1.0
-0.5
0.0
0.5
ln Cv,tt

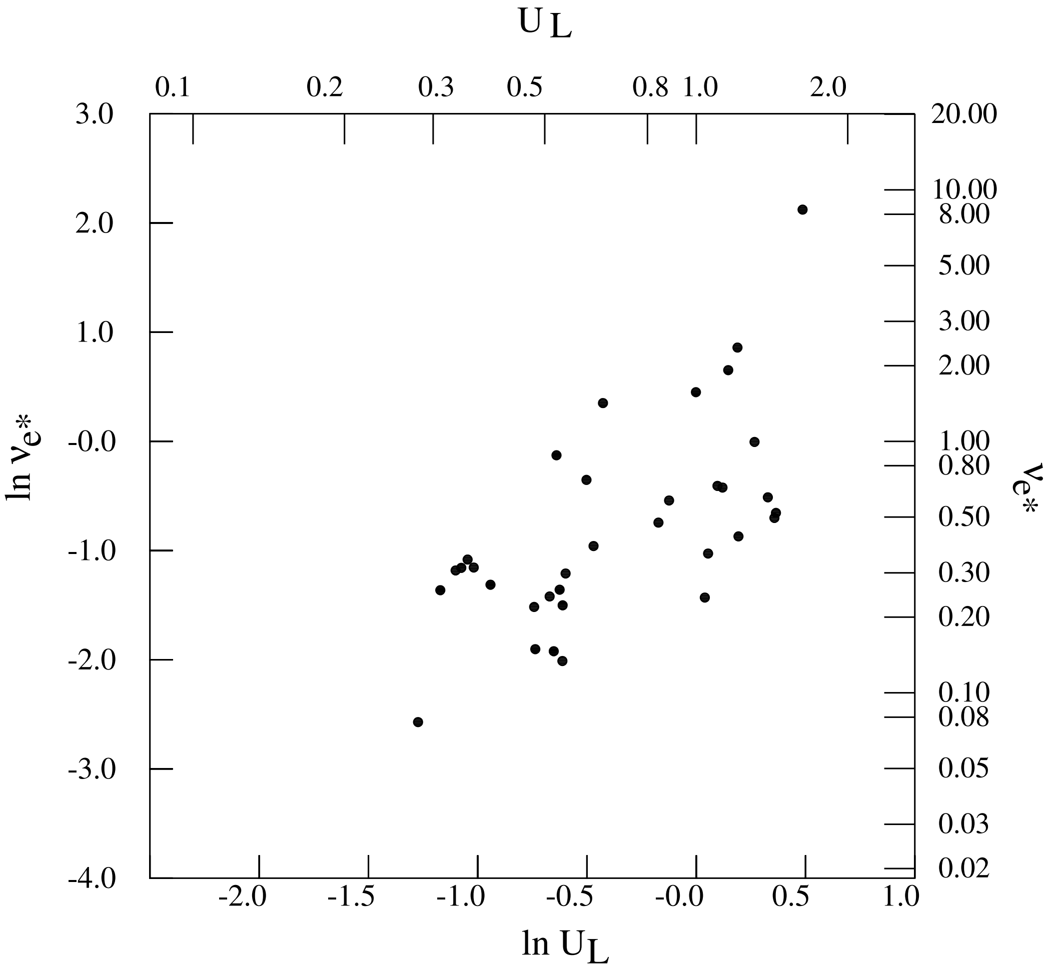

U L
0.1
0.2
0.3
0.5
0.8
1.0
2.0
3.0
2.0
1.0
-0.0
-1.0
-2.0
-3.0
-4.0
ln ve*
20.00
10.00
8.00
5.00
3.00
2.00
1.00
0.80
0.50
0.30
0.20
0.10
0.08
0.05
0.03
0.02
ve*
-2.0
-1.5
-1.0
-0.5
-0.0
0.5
1.0
ln U L

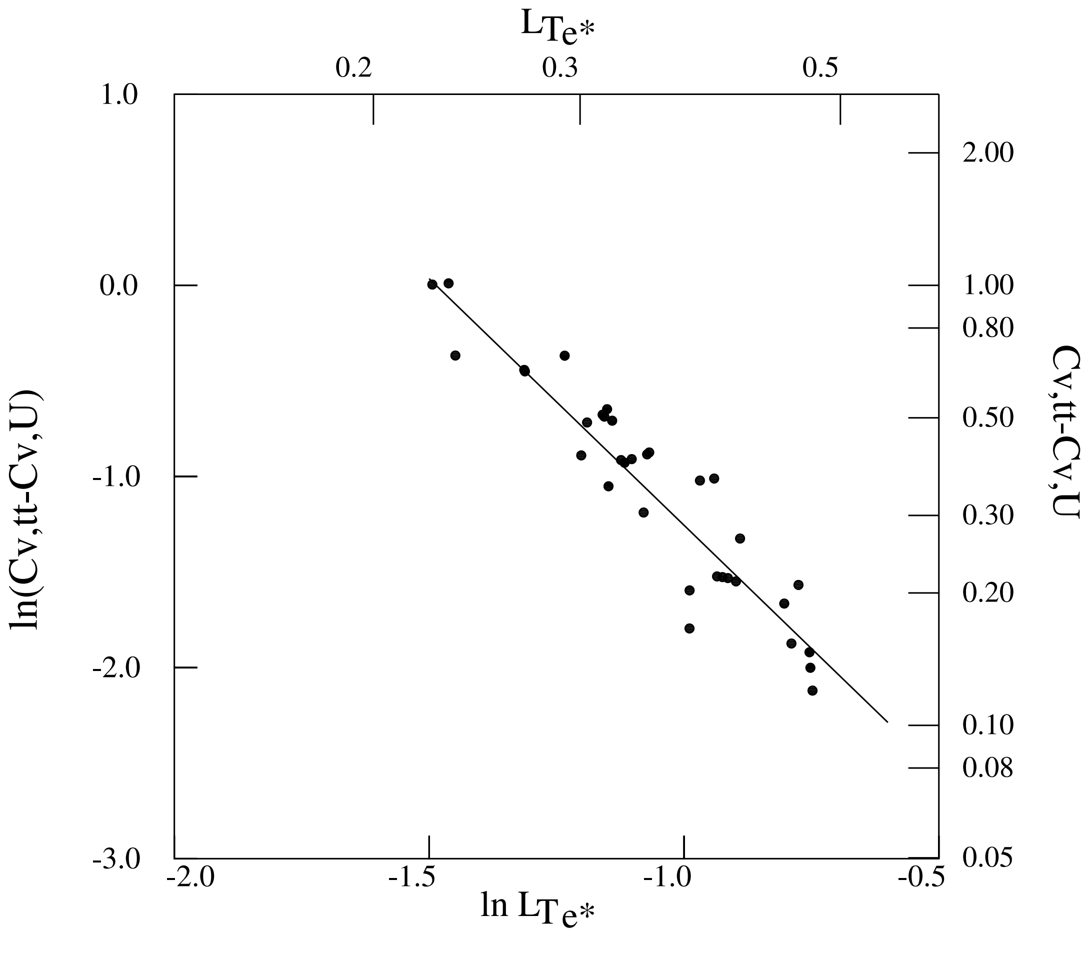
L Te*
0.2
0.3
0.5
1.0
0.0
-1.0
-2.0
-3.0
2.00
1.00
0.80
0.50
0.30
0.20
0.10
0.08
0.05
ln(Cv,tt-Cv,U)
Cv,tt-Cv,U
-2.0
-1.5
-1.0
-0.5
ln L Te*

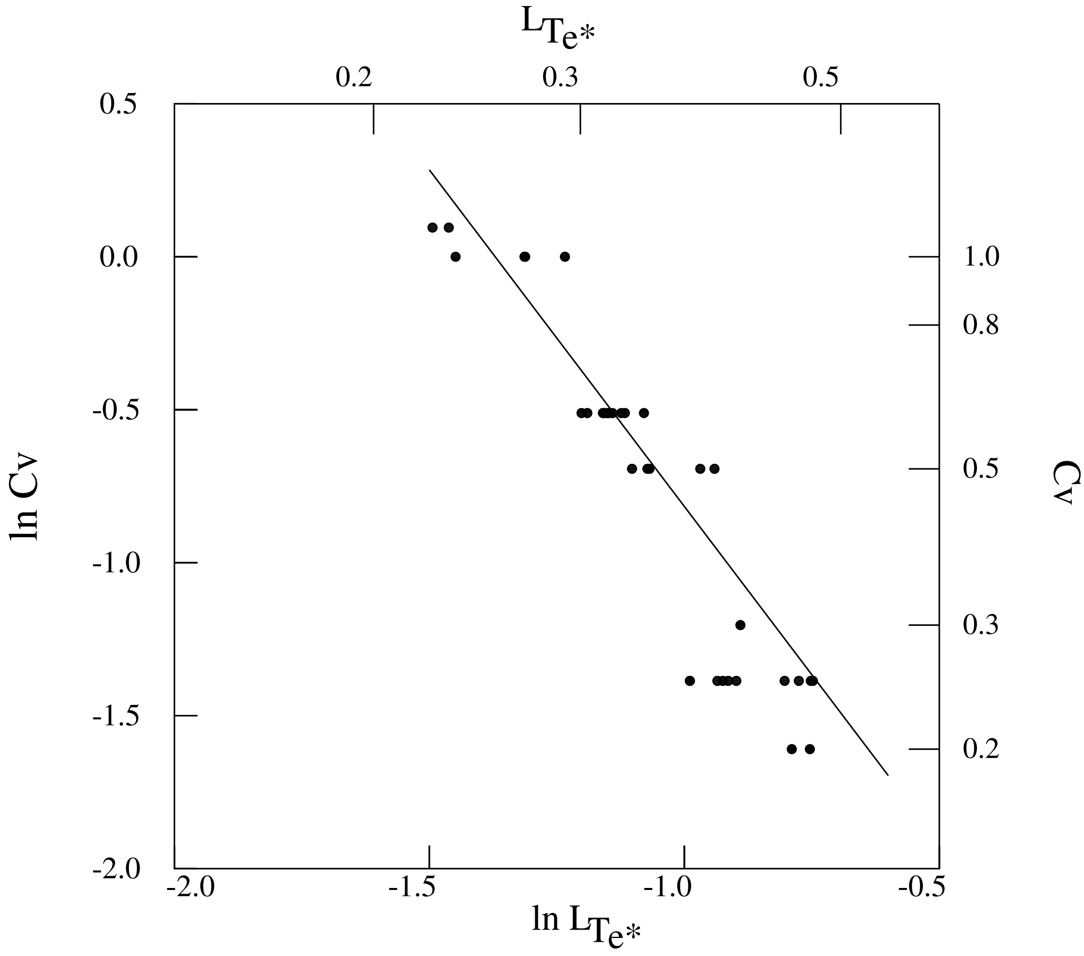

L_{Te*}
0.2
0.3
0.5
0.5
0.0
-0.5
-1.0
-1.5
-2.0
ln Cv
1.0
0.8
0.5
0.3
0.2
Cv
-2.0
-1.5
-1.0
-0.5
ln L_{Te*}